*energies*

MDPI

*Article*

# Assessment of the Actual and Required Cooling Demand for Buildings with Extensive Transparent Surfaces

**Attila Kostyák, Szabolcs Szekeres * and Imre Csáky ***

Department of Building Services and Building Engineering, Faculty of Engineering, University of Debrecen, Ótemető Str. 2-4, 4028 Debrecen, Hungary; kostyak.attila@eng.unideb.hu
* Correspondence: szekeres@eng.unideb.hu (S.S.); imrecsaky@eng.unideb.hu (I.C.)

**Abstract:** Energy consumption in buildings with large, glazed facades rises markedly in the summer, driven by cooling demands that vary with structural characteristics and external climate conditions. This study is unique in examining daily cooling needs in lightweight and heavyweight constructions, utilizing meteorological data from 782 summer days in Debrecen, Hungary. Unlike standard approaches, which often overlook localized meteorological variables, this analysis focuses on actual "clear sky" scenarios across distinct summer day types: normal, hot, and torrid. The findings indicate that orientation and construction type significantly affect cooling demands, with east-facing rooms demanding up to 14.2% more cooling in lightweight structures and up to 35.8% in heavyweight structures during peak hours (8 a.m. to 4 p.m.). This study reveals that for west-facing facades, extending use beyond 4 p.m. markedly increases energy loads. Furthermore, the cooling demand peak for heavyweight buildings occurs later in the day, driven by their higher thermal capacity. These insights underscore the importance of aligning HVAC system design with operational schedules and building orientation, offering data-driven strategies to enhance energy efficiency in buildings with diverse thermal and solar exposure profiles.

**Keywords:** operative temperature; cooling demand; hottest days; global radiation



**Citation:** Kostyák, A.; Szekeres, S.; Csáky, I. Assessment of the Actual and Required Cooling Demand for Buildings with Extensive Transparent Surfaces. *Energies* **2024**, *17*, 5814. https://doi.org/10.3390/en17235814

Academic Editor: Alessandro Cannavale

Received: 22 October 2024
Revised: 11 November 2024
Accepted: 13 November 2024
Published: 21 November 2024



## 1. Introduction

Improving the energy performance of buildings is an aim that modern engineering must take into consideration. This can be achieved by improving the building envelopes and the equipment used or via an efficient operation strategy required to save as much energy as possible while maintaining the comfort levels in the building. The increased comfort needs of occupants and standards expectations generate higher energy consumption. To maintain the operative temperature in buildings during the summer, energy input is required. To design a cooling system for a building, first, a cooling load calculation is needed. Several factors must be taken into consideration when determining the cooling load of a building, such as the structure of the building, the internal heat sources, the intensity of solar radiation, and the external air temperature. The design methods in current standards use statistical meteorological data for calculating the cooling demand under a specific set of assumed conditions [1–4]. This study analyzed data from actual days and compared the direct solar radiation values between the actual days and the values given by different standards. To be able to design the right cooling system for the summer period, it is important to have information about the local climate. The number and properties of heat waves (the number of summer, hot, and torrid days) have a great effect on the energy consumption of the cooling system. Due to climate change, the number and length of heat waves will increase. The effect of climate change impacts the energy demand of buildings [5]. This is a significant issue as the final energy consumption of buildings reaches 39% of the total energy consumption in the EU, which includes the energy consumption by the cooling systems [6]. Several studies have examined the impact of climate change on

building energy consumption, particularly focusing on heating and cooling requirements in different regions, such as Australia and Taiwan [7,8]. Simulations have been made to predict the future (2040–2070) energy demand [9]. If the hourly global (direct and diffuse) radiation values and the daily mean air temperature values are known, an appropriate operation strategy can be developed, and we can also determine the appropriate sizing of the equipment to reduce the energy consumption of the building [10,11]. In a building, it is necessary to examine how the heat load caused by transparent surfaces develops during the day. The heat gained through fenestration (exterior glass walls or windows) during summer days leads to a high indoor temperature, which can be reduced by managing the sum of heat gained through transparent elements with shading or by using cooling equipment [12]. As solar radiation has an immense effect on the heat load, it requires further investigation. In this paper, horizontal global radiation data were collected for 11 years (2009–2019) in Debrecen (Hungary). The diffuse and direct radiation values were determined for four different orientations of the vertical building facades. During the investigation, a summer, hot, and torrid day were chosen from the collected data. Using these data, the heat load was calculated for an example building. The choice of the example building was based on buildings in which the transparent surfaces reach at least 50% of the external surfaces. The aim of this article is to present the progression of the building's thermal load under given meteorological conditions, taking into account the operating temperature and thermal mass. The primary objective is to examine the influence of the orientation of transparent surfaces; the building materials; the operational hours of the building, especially in the peak occupancy time; the operative temperature (across various comfort categories) using actual climatic data; and the cooling demand using validated calculation methods. Based on this analysis, conclusions will be drawn regarding the cooling heat generation and dissipation system, and recommendations will be provided for building operation considering the operational interval of the building. Validation of the methods was conducted according to the following articles [13–16]. To ensure the reliability of the methods applied in this study, the cooling load calculation methods were validated by comparing them with established benchmarks and empirical data. This validation process ensures that the cooling load estimates are both accurate and applicable to buildings with extensive glazing.

## 2. Material and Methods

The Great Hungarian Plain is located in the heart of the Carpathian Basin in south-eastern Hungary (see Figure 1). This region is characterized by its low-lying terrain, with elevations ranging from 75 to 180 m above sea level, resulting in a relatively flat topography. The annual mean precipitation ranges from 500 to 550 mm, while the average temperature is between 10 and 11 °C. Summers are generally characterized by sunshine and warmth, with average temperatures exceeding 20 °C. In contrast, winters are cold, with temperatures averaging around −2 °C, frequently accompanied by snowfall. This considerable annual temperature fluctuation, exceeding 20 °C, can be attributed to the continental climate influence prevailing in the eastern region of Hungary. The overall annual mean temperature is approximately 10 °C [17].

Typically, wind velocity in the area registers at around 3 m/s, with a prevailing northeasterly wind direction. Debrecen (47.5° N, 21.5° E), positioned at an elevation of 120 m above sea level within the predominantly flat terrain of the Great Hungarian Plain (Figure 1), is particularly conducive to the development of the Urban Heat Island (UHI) effect. It stands as Hungary's second-largest city, boasting a population of 220,000 residents. Debrecen serves as a pivotal hub for cultural, academic, and economic activities within the country's northeastern region. The city and its surrounding environs fall within Köppen's climate classification as region Cfb [18]. Hourly horizontal global radiation data and mean outdoor temperature were provided by the local Agro-Meteorological Observatory for the years 2009 to 2019. The outdoor dry-bulb air temperature was measured at a height of 2.0 m. The temperature sensor used was a Pt100-1/10 with ±0.1 °C accuracy. The global

solar radiation was measured with a Kipp and Zomen CMP-11 sensor with ±1% accuracy [14].

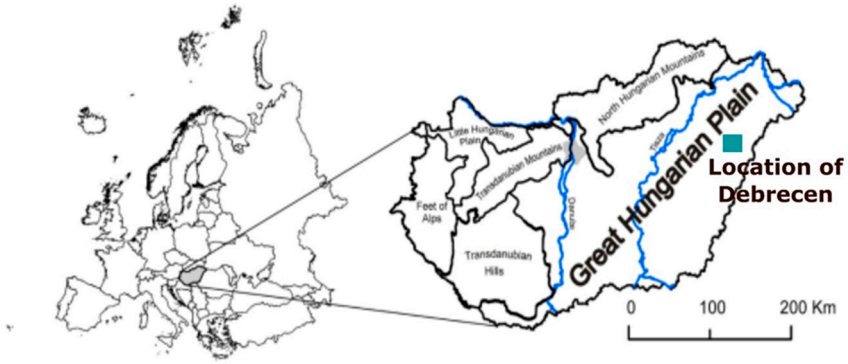


**Figure 1.** The Great Hungarian Plain [18].

### *2.1. Hottest Days, Heat Waves*

In Table 1, we can see the definition of the hottest days according to the Hungarian Meteorological Service.

**Table 1.** Hottest days definition according to the Hungarian Meteorological Service [19].

| | | |
|---|---|---|
| Hottest Days | Summer | $T_{max} > 25$ °C |
| | Hot | $T_{max} \geq 30$ °C |
| | Torrid | $T_{max} \geq 35$ °C |

For the analyzed period of 11 years, the number of summer days, hot days, and torrid days are presented in Table 2.

**Table 2.** Hottest days in the 2009–2019 period.

| Year | Summer Days | Hot Days | Torrid Days |
|---|---|---|---|
| 2009 | 51 | 22 | 0 |
| 2010 | 40 | 18 | 0 |
| 2011 | 41 | 19 | 1 |
| 2012 | 40 | 31 | 9 |
| 2013 | 50 | 20 | 3 |
| 2014 | 47 | 16 | 0 |
| 2015 | 36 | 32 | 7 |
| 2016 | 50 | 11 | 0 |
| 2017 | 49 | 24 | 1 |
| 2018 | 68 | 25 | 0 |
| 2019 | 42 | 29 | 0 |

Table 2 shows that in the examined years, there were 782 days when the maximum temperature was 25 °C or higher. The Meteorological Observatory is based on the outskirts of Debrecen in an open field. In the city, the external temperature can be higher due to the urban heat island effect [20]; this can influence the number of summer, hot, and torrid days. Table 3 presents the external maximum air temperature frequency in the investigated period.

**Table 3.** Outdoor maximum temperatures in the analyzed period (2009–2019).

| Daily Maximum, °C | Number of Days |
|---|---|
| 25–25.99 | 106 |
| 26–26.99 | 105 |
| 27–27.99 | 121 |
| 28–28.99 | 91 |
| 29–29.99 | 91 |
| 30–30.99 | 76 |
| 31–31.99 | 67 |
| 32–32.99 | 48 |
| 33–33.99 | 34 |
| 34–34.99 | 22 |
| 35–35.99 | 14 |
| 36–36.99 | 5 |
| 37–37.99 | 2 |

According to the World Meteorological Organization, a heat wave is defined as an extended period (five or more days), where the daily maximum temperature is higher by 5 °C or more than the daily average maximum temperature [21]. In Table 4, the criteria of heat waves according to the Hungarian Meteorological Service are presented.

**Table 4.** Heat waves definition according to the Hungarian Meteorological Service [19].

| | | |
|---|---|---|
| Heat waves | Level 1 | $T_{mean} \geq 25$ °C 1–2 day |
| | Level 2 | $T_{mean} \geq 25$ °C 3 days at least or ≥27 °C 1 day at least |
| | Level 3 | $T_{mean} \geq 27$ °C 3 days or more |

For the analyzed period, the number of heat waves with different levels are shown in Table 5.

**Table 5.** Heat waves in the analyzed period.

| | Level 1 | Level 2 | Level 3 |
|---|---|---|---|
| 2009 | 6 | 1 | 0 |
| 2010 | 3 | 2 | 0 |
| 2011 | 2 | 2 | 0 |
| 2012 | 2 | 4 | 1 |
| 2013 | 2 | 3 | 0 |
| 2014 | 1 | 0 | 0 |
| 2015 | 4 | 4 | 2 |
| 2016 | 1 | 1 | 0 |
| 2017 | 4 | 2 | 0 |
| 2018 | 8 | 0 | 0 |
| 2019 | 5 | 1 | 0 |

As can be seen between 2009 and 2019, 38 heat waves of level 1, 20 heat waves of level 2, and 3 heat waves of level 3 were registered. To validate the calculation model of the solar

radiation, a summer day was selected from heat wave level 1, when the global radiation was 8110.21 Wh/m$^2$ day. The maximum measured global radiation was 926.83 W/m$^2$, while the maximum daily external air temperature was 25.3 °C.

### 2.2. Calculation Method of Direct and Diffuse Radiation on Horizontal Surfaces

As we obtained the hourly horizontal global radiation values measured by the Meteorological Observatory for a summer day, we were able to determine the diffuse radiation on horizontal surfaces using the method developed by Erbs et al. using Equations (1) and (2) [22].

$$\begin{array}{lll} \frac{I_{DifH}}{I_{GH}} = 1 - 0.9k_T & for & k_T \leq 0.22 \\ \frac{I_{DifH}}{I_{GH}} = 0.9511 - 0.160k_T + 4.388k_T^2 - 16.638k_T^3 + 12.336k_T^4 & for & 0.22 < k_T \leq 0.8 \\ \frac{I_{DifH}}{I_{GH}} = 0.165 & for & k_T > 0.8 \end{array} \quad (1)$$

The clearness index can be obtained using Equation (2):

$$k_T = \frac{I_{GH}}{G_{SC} cos\theta_z}. \quad (2)$$

The solar constant is $G_{SC}$ = 1367 W/m$^2$ [14,22–27].

The direct solar radiation on horizontal surfaces ($I_{difH}$) can be determined using Equation (3) [22–25]:

$$I_{dirH} = \frac{I_{GH} - I_{difH}}{cos\theta_z}. \quad (3)$$

Radiation values measured on cloudy days need to be converted to those of clear sky days as direct radiation values are higher than for actual days, while the diffuse radiation values are lower. Using Equations (1)–(3), the raw radiation values were adjusted to represent clear sky conditions, as shown in Table 6. In Table 6, we can see the measured global radiation ($I_{GH}$), the calculated direct radiation on horizontal surfaces ($I_{dirH}$), and the obtained diffuse radiation ($I_{difH}$) on horizontal surfaces for the selected summer day. Table 6 also contains the adjusted data to clear sky day.

**Table 6.** Global, direct, and diffuse radiation on a horizontal surface for 24 h.

| Hour | $I_{GH}$ | $I_{dirH}$ | $I_{difH}$ | $I_{dirH}$ | $I_{difH}$ |
|---|---|---|---|---|---|
| | | Raw Data | | Data Adjusted to Clear Sky Day | |
| | | W/m$^2$ | | | |
| 0:00 | 0.00 | 0.00 | 0.00 | 0.00 | 0.00 |
| 1:00 | 0.00 | 0.00 | 0.00 | 0.00 | 0.00 |
| 2:00 | 0.00 | 0.00 | 0.00 | 0.00 | 0.00 |
| 3:00 | 0.00 | 0.00 | 0.00 | 0.00 | 0.00 |
| 4:00 | 0.00 | 0.00 | 0.00 | 0.00 | 0.00 |
| 5:00 | 56.30 | 56.30 | 0.00 | 47.01 | 9.29 |
| 6:00 | 205.12 | 98.47 | 106.65 | 171.27 | 33.84 |
| 7:00 | 377.98 | 122.55 | 255.43 | 315.62 | 62.37 |
| 8:00 | 546.03 | 138.34 | 407.69 | 455.94 | 90.10 |
| 9:00 | 697.82 | 148.57 | 549.25 | 582.68 | 115.14 |
| 10:00 | 818.43 | 156.65 | 661.78 | 683.39 | 135.04 |
| 11:00 | 897.33 | 162.03 | 735.30 | 749.27 | 148.06 |
| 12:00 | 926.83 | 163.39 | 763.45 | 773.91 | 152.93 |

**Table 6.** *Cont.*

| Hour | $I_{GH}$ | $I_{dirH}$ | $I_{difH}$ | $I_{dirH}$ | $I_{difH}$ |
|---|---|---|---|---|---|
| | | Raw Data | | Data Adjusted to Clear Sky Day | |
| | | $W/m^2$ | | | |
| 13:00 | 900.83 | 160.67 | 740.16 | 752.20 | 148.64 |
| 14:00 | 753.03 | 206.30 | 546.74 | 628.78 | 124.25 |
| 15:00 | 712.12 | 139.36 | 572.75 | 594.62 | 117.50 |
| 16:00 | 568.77 | 120.39 | 448.38 | 474.92 | 93.85 |
| 17:00 | 375.95 | 124.50 | 251.45 | 313.92 | 62.03 |
| 18:00 | 218.87 | 86.31 | 132.55 | 182.75 | 36.11 |
| 19:00 | 54.79 | 54.79 | 0.00 | 45.75 | 9.04 |
| 20:00 | 0.00 | 0.00 | 0.00 | 0.00 | 0.00 |
| 21:00 | 0.00 | 0.00 | 0.00 | 0.00 | 0.00 |
| 22:00 | 0.00 | 0.00 | 0.00 | 0.00 | 0.00 |
| 23:00 | 0.00 | 0.00 | 0.00 | 0.00 | 0.00 |

### *2.3. Converting Horizontal Radiation Values to Vertical Radiation Values Using the Rb Factor*

Basunia et al. defined the ratio of direct radiation on the tilted surface to a horizontal surface as the geometric factor, and it is a crucial parameter in solar energy modeling and design calculations. Geometric factors ($R_b$) and different parameters usually are expressed as follows [25,27,28]:

$$R_b = \frac{cos\theta}{cos\theta_z}, \tag{4}$$

where:

$$cos\theta = sin\delta sin\phi cos\beta - sin\delta cos\phi sin\beta cos\gamma + cos\delta cos\phi cos\beta cos\omega + cos\delta sin\phi sin\beta cos\gamma cos\omega + cos\delta sin\beta sin\gamma sin\omega \tag{5}$$

and

$$cos\theta_z = sin\delta sin\phi + cos\delta cos\phi cos\omega cos\theta_z = sin\delta sin\phi + cos\delta cos\phi cos\omega. \tag{6}$$

The validation of the calculation method based on the Bogoslovskij report is presented in a previous published article [18,28,29]. Using Equations (4)–(6), the hourly values of the geometric factor were calculated for the selected summer day. In our case, for the selected summer day, the variation of the Rb factor for different orientations of a vertical wall is presented in Figure 2.

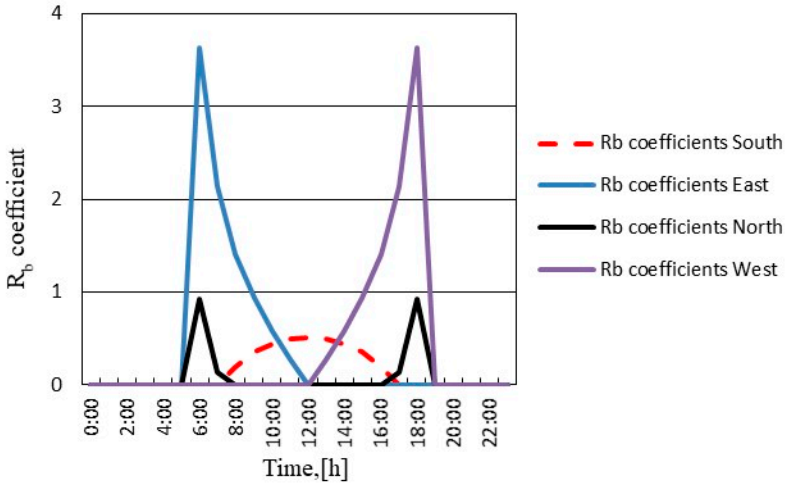


**Figure 2.** Daily variation of $R_b$ values for different orientations of the wall on a summer day.

### 2.4. Diffuse and Direct Radiation on Vertical Surfaces

The validation of the calculation method of hourly solar radiation incidents on an inclined surface is presented in a previously published article [14]. The values of the above-mentioned parameters have been calculated from the available global solar radiation data measured on a horizontal surface. Norris stated that the diffuse solar radiation on a tilted surface can be determined with Equations (7) and (8) [30–32].

$$I_{difβ}^{iso} = R_β I_{difh} I_{difβ}^{iso} = R_β I_{difh}, \quad (7)$$

where:

$$R_β = \frac{1 + cosβ}{2}. \quad (8)$$

The results in Table 7 provide the calculated diffuse radiation values on a vertical surface over a 24-h period, which are essential for assessing the performance of the model under varying atmospheric conditions.

**Table 7.** Calculated values of the diffuse radiation on a vertical surface for 24 h.

| Hour | $I_{difβ}^{iso}$ | $I_{difβ}^{iso}$ |
|---|---|---|
| | Actual Day | Clear Sky Day |
| | W/m$^2$ | |
| 0:00 | 0.00 | 0.00 |
| 1:00 | 0.00 | 0.00 |
| 2:00 | 0.00 | 0.00 |
| 3:00 | 0.00 | 0.00 |
| 4:00 | 0.00 | 0.00 |
| 5:00 | 28.15 | 4.64 |
| 6:00 | 49.23 | 16.92 |
| 7:00 | 61.27 | 31.18 |
| 8:00 | 69.17 | 45.05 |
| 9:00 | 74.28 | 57.57 |
| 10:00 | 78.33 | 67.52 |
| 11:00 | 81.01 | 74.03 |
| 12:00 | 81.69 | 76.46 |
| 13:00 | 80.34 | 74.32 |
| 14:00 | 103.15 | 62.13 |
| 15:00 | 69.68 | 58.75 |
| 16:00 | 60.20 | 46.92 |
| 17:00 | 62.25 | 31.02 |
| 18:00 | 43.16 | 18.06 |
| 19:00 | 27.40 | 4.52 |
| 20:00 | 0.00 | 0.00 |
| 21:00 | 0.00 | 0.00 |
| 22:00 | 0.00 | 0.00 |
| 23:00 | 0.00 | 0.00 |

Direct solar radiation was determined using Equation (9).

$$I_{dir\beta} = R_b I_{dirH} \quad (9)$$

For the selected summer day, the direct solar radiation values summing different orientations of a vertical wall are presented in Figure 3.

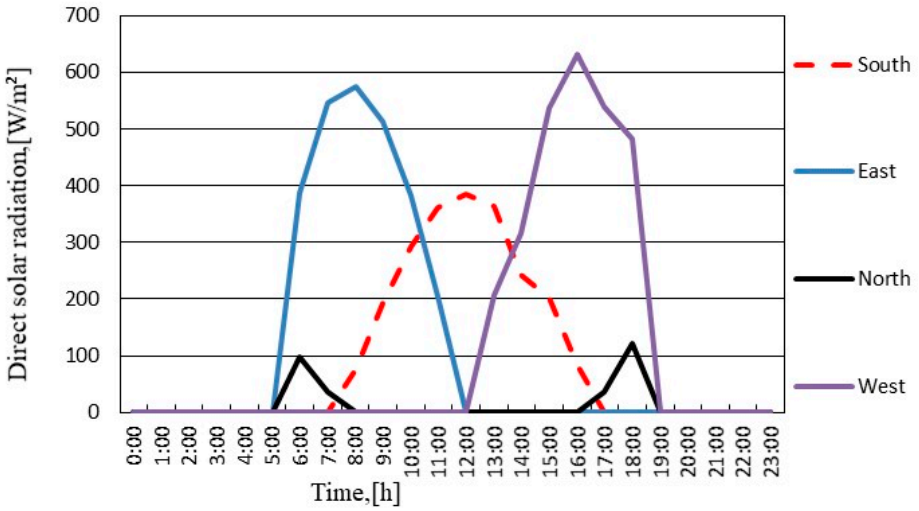


**Figure 3.** Direct solar radiation values.

In Table 8, the daily incident solar energy yield is presented for the selected summer day, which was calculated both for horizontal and vertical surfaces with different orientations.

**Table 8.** Energy yield calculation for a summer day [Wh/m$^2$ day].

| | Horizontal Surface | | Vertical Surface | | | | |
|---|---|---|---|---|---|---|---|
| | **Diffuse** | **Direct** | **Diffuse** | **South** | **East** | **West** | **North** |
| Actual day | 1938.62 | 6171.59 | 969.31 | 2197.24 | 2611.79 | 2711.35 | 292.37 |
| Clear sky day | 1338.18 | 6772.02 | 669.09 | 2294.5 | 3091.11 | 3136.26 | 415.65 |

### *2.5. Summer, Hot, and Torrid Day Data for the Calculation of the Cooling Load*

This study identified the heat waves during each year separately for the summer period from which the selected days were chosen for cooling load calculation. The summer day was chosen from heat wave level 1, the hot day from heat wave level 2 and the torrid day from heat wave level 3. On the selected summer, hot, and torrid days, the maximum daily external air temperatures were 25.3 °C, 32.4 °C, and 35.6 °C. The calculations were undertaken for clear sky days as the cloudy sky has a major influence on the direct and diffuse radiation values [33].

As can be seen in Figure 4, the maximum external air temperature on the selected days and the temperatures used by the Romanian National Institute for Research and Development are higher than the values given by the MSZ 04-140 standard, except for the summer day [34,35].

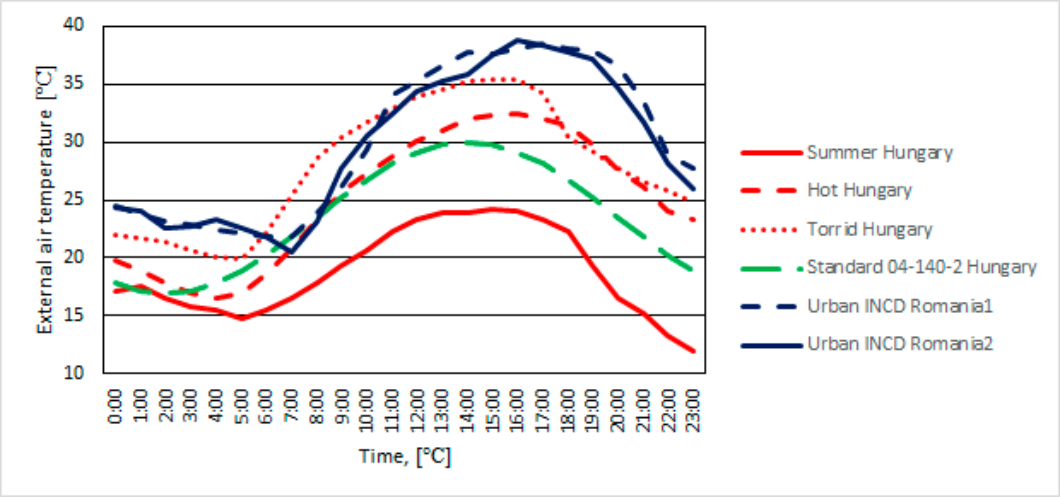


**Figure 4.** Comparison of design days by external air temperature.

Analyzing Figure 5, it can be stated that the energy yield of actual days, except for the north orientation, is higher than the values in the standards; hence, the cooling load is higher. If the calculation is based only on the standards values, the cooling system might be undersized.

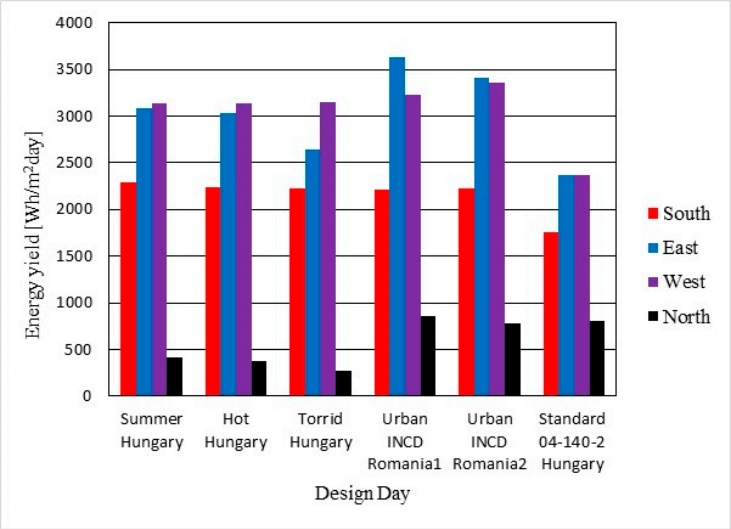


**Figure 5.** Comparison of design days by energy yield.

## 3. Results and Discussion

The cooling load examination in the present paper was conducted on an example building that is three storeys high. The rooms examined are corner rooms on the top floor. This floor has the highest heat gains (due to lack of natural shading) and solar radiation compared to the other floors. The rooms are identical in size, with the following dimensions: 4.8 m (l) × 4.8 m (w) × 3 m (h) ceiling height. The only difference in the rooms is the orientation of transparent surfaces (north, south, west, and east). Each room has two external sides, and one of them is fenestration.

The thermal transmittance values of the building's external composite structures were calculated or given by the manufacturer; they are presented in Table 9.

**Table 9.** Thermal transmittance values.

| Structures | U [W/m$^2$ K] |
|---|---|
| Wall | 0.226 |
| Window | 1 |
| Flat roof | 0.166 |

The windows' solar energy transmittance value is g = 0.7 and has no shading, as can be seen in Figure 6. Figure 6 presents two images side by side: one depicting an actual building and the other featuring a fictitious structure. The inclusion of both images serves the purpose of illustrating that such architectural designs exist in reality. The frame of the window is considered 15% of the total glazed area. The air change rate in the calculation was set to 0.5 h$^{-1}$.

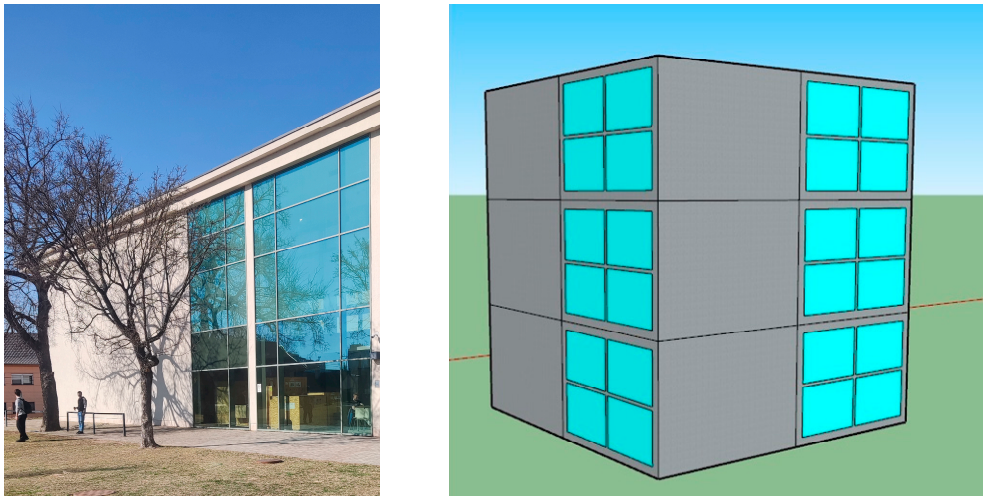

**Figure 6.** Example building.

Both light- and heavyweight constructions were analyzed. A building is considered lightweight according to Hungarian regulations if the specific thermal mass per square meter is equal to or lower than 400 kg. If the specific thermal mass is higher than 400 kg, then it is considered a heavyweight construction. The weight of the building influences the thermal capacity. Thus, two cases were examined. The first case is a heavyweight construction with C = 14,969.9 kJ/K thermal capacity, and the second case is a lightweight construction with C = 3030.5 kJ/K thermal capacity.

The calculation was undertaken according to the EN ISO 13790:2008 standard. The used meteorological data were presented above in the Material and Methods section. No internal heat gains were taken into consideration as the study focused on external heat gains. The RC network and the validation of the model in Figure 7 are presented thoroughly in reference [13,19].

The thermal comfort requirements in enclosed spaces according to the MSZ CR 1752: 2000 standard [36], which defines the recommended operative temperature ranges for different comfort categories, are as follows: for Category A, which represents high comfort levels, the standard recommends an operative temperature of between 23.5 °C and 25.5 °C; for Category B, aimed at medium comfort, the standard specifies an operative temperature of between 23 °C and 26 °C; and for Category C, representing basic comfort, the target is between 22 °C and 27 °C. These values were selected based on the standard's guidelines to ensure compliance with established thermal comfort criteria. The operative temperature was set at 23.5 °C for Category A, 26 °C for Category B, and 27 °C for Category C. Table 10 shows the maximum operative temperature for each category.

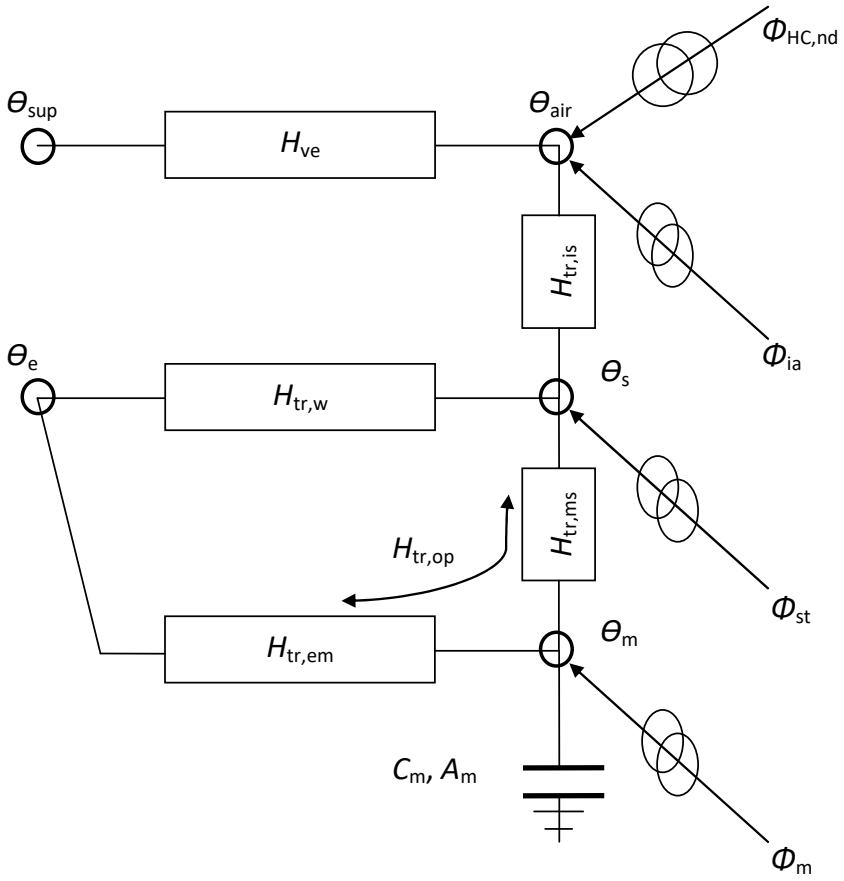


**Figure 7.** RC network heat flows [4].

**Table 10.** Comfort categories according to standards MSZ CR 1752: [36].

| Comfort Categories | Operative Temperature [°C] Summer (Cooling) |
|---|---|
| A | 24.5 ± 1.0 |
| B | 24.5 ± 1.5 |
| C | 24.5 ± 2.5 |

The operative temperature is calculated using Equation (10) [36].

$$\Theta_{op} = (\Theta_s \cdot 0.7) + (\Theta_{air} \cdot 0.3), \quad (10)$$

where:

$\Theta_{op}$—operative temperature;

$\Theta_s$—surface temperature;

$\Theta_{air}$—air temperature.

This equation is essential for determining the effective temperature experienced by occupants, which combines radiant and air temperatures. Although this calculation is not explicitly shown in the results, it was applied to determine the initial operative temperatures used in our analysis.

Table 11 shows the total cooling peak performance required for the given buildings while sustaining different levels of comfort. Table 11 shows that there is a significant difference between the cooling peak performance requirements of light and heavyweight buildings. This is due to the different thermal capacities of the structures. As the thermal resistances of the structures are the same, the difference between the building structures

is how the direct solar gain is handled. Based on the above, in a lightweight building, the operative temperature is more sensitive to direct solar gain than in a heavyweight construction. This statement is also supported by Figure 8b, which shows that in the room with the glazed surface at a north orientation, there is little difference between the lightweight and heavyweight construction in terms of the heat load. In contrast, in Figure 8c–e, we can see that a large heat load difference develops between the two types of construction during the extensive sunny hours.

**Table 11.** Cooling demand of analyzed floor on heavyweight and lightweight construction [W].

| | **Heavyweight Construction** | | | **Lightweight Construction** | | |
|---|---|---|---|---|---|---|
| **Operative Temperature** | **A** $T_{op}$**: 23.5 °C** | **B** $T_{op}$**: 26.0 °C** | **C** $T_{op}$**: 27.0 °C** | **A** $T_{op}$**: 23.5 °C** | **B** $T_{op}$**: 26.0 °C** | **C** $T_{op}$**: 27.0 °C** |
| Summer day | 13,122 | 8173 | 6393 | 21,946 | 19,693 | 18,793 |
| Hot day | 14,619 | 9800 | 7902 | 23,893 | 21,641 | 20,738 |
| Torrid day | 14,963 | 10,201 | 8303 | 24,147 | 21,901 | 21,007 |

Figure 8a is an aggregate of diagrams Figure 8b–e. The peak time (8 a.m.–4 p.m.) was marked in the diagrams. This period is considered the active time, for example, in office buildings, educational institutes, government institutes, etc. It can be seen in the diagrams that the maximum cooling demand during the peak time only reaches the east-facing room for both types of construction and the south-facing room for lightweight construction. In absolute terms, the heat load on the west-facing room is higher; however, it does not reach its maximum during peak time. This knowledge can be used to design the cooling system. To fit the cooling emitters properly to the heat load of the room in the case of west-facing rooms, it is worthwhile installing cooling equipment with asymmetrical performance. This conclusion also applies to the south-facing rooms. In the case of the east-facing offices, the heat load is significant throughout the peak time, so an even distribution of the cooling emitters can be recommended there. In the case of the north-facing rooms, the difference in heat load as a function of the outdoor conditions is approximately the same as the change in the outside temperature of the sample day. In the case of rooms facing south, east, and west, due to the significant global radiation, the heat load of lightweight and heavyweight buildings differs significantly in the period of high global radiation reaching the glazed surfaces. According to each orientation, the radiation on the glazed surfaces occurs at different times, so the highest global radiation value appears in the east at the earliest and in the west at the latest.

Based on Table 12, the heat load of the east- and west-facing rooms is the highest, and the cooling capacity requirement of the lightweight rooms is significantly higher than that of the heavyweight structured rooms. If each room has an individual cooling system, then those need to be sized according to the values found in Table 12. The building's required cooling demand is lower than the sum of the rooms' maximum cooling demand because the heat load in the rooms does not occur at the same time. This fact can be used when designing a central cooling system. Figure 9 shows the required cooling demand of the rooms and the aggregated curve of the heat load of the buildings. Figure 9 presents the time course of the cooling demand in the case of light- and heavyweight construction on summer, hot, and torrid days. The heat load of the rooms with different structures is summarized in Figure 9 by orientation and absolute value.

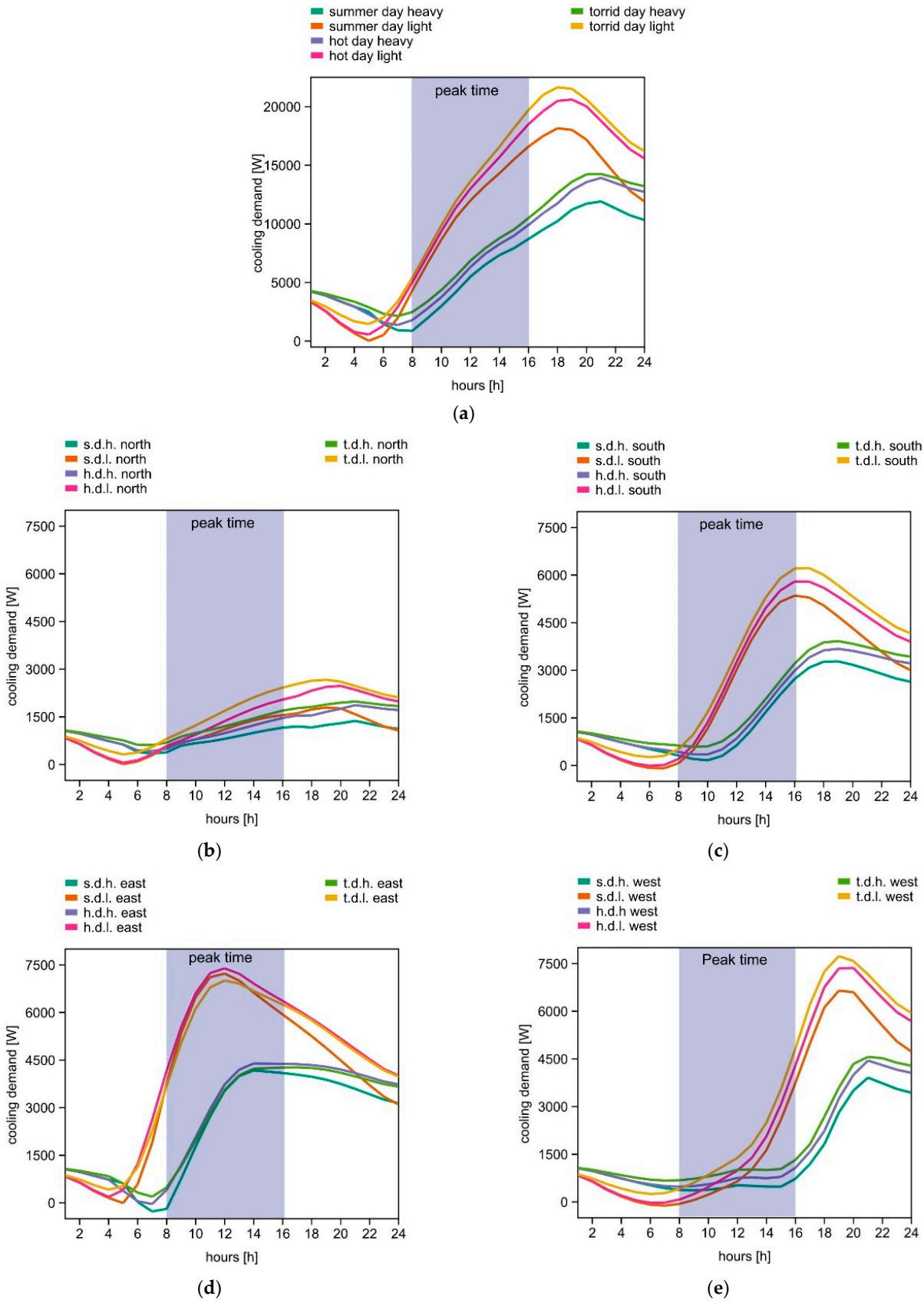


**Figure 8.** (**a**) Summarized cooling demand. (**b**–**e**) Cooling demand of a room with the transparent surface facing (**b**) north, (**c**) south, (**d**) east, and (**e**) west.

**Table 12.** Maximum cooling demand for the rooms [W].

| | | Heavy Construction | | | | Light Construction | | | |
|---|---|---|---|---|---|---|---|---|---|
| **Comfort Category** | **Operative Temperature** | **South** | **North** | **East** | **West** | **South** | **North** | **East** | **West** |
| A $T_{op}$: 23.5 °C | summer day | 3361 | 1458 | 4212 | 4091 | 5462 | 1938 | 7398 | 7148 |
| | hot day | 3715 | 1914 | 4402 | 4588 | 5908 | 2581 | 7555 | 7849 |
| | torrid day | 3979 | 2035 | 4281 | 4668 | 6319 | 2738 | 7167 | 7923 |
| B $T_{op}$: 26.0 °C | summer day | 2138 | 296 | 2810 | 2929 | 4900 | 1417 | 6749 | 6627 |
| | hot day | 2495 | 752 | 3127 | 3426 | 5346 | 2060 | 6907 | 7328 |
| | torrid day | 2755 | 873 | 3039 | 3534 | 5763 | 2217 | 6519 | 7402 |
| C $T_{op}$: 27.0 °C | summer day | 1648 | 0 | 2281 | 2464 | 4675 | 1209 | 6490 | 6419 |
| | hot day | 2018 | 287 | 2636 | 2961 | 5121 | 1851 | 6647 | 7119 |
| | torrid day | 2266 | 408 | 2549 | 3080 | 5545 | 2009 | 6260 | 7193 |

It can be seen in Figure 9 that the aggregated curve of the heat load does not reach the maximum value during the peak time (8 a.m.–4 p.m.). In the case of light construction buildings, the maximum heat loads in the peak time are significantly closer to the absolute maximum value compared to heavyweight construction buildings.

Tables 13 and 14 illustration these characteristics. Based on Table 13, it can be seen that the required cooling demand of the top floor is 18.2% higher on a torrid day than on a summer day. This means that certain standards, such as 04-140-02 [35], which use a summer day for cooling demand calculation, can underestimate the cooling demand on hot and torrid days.

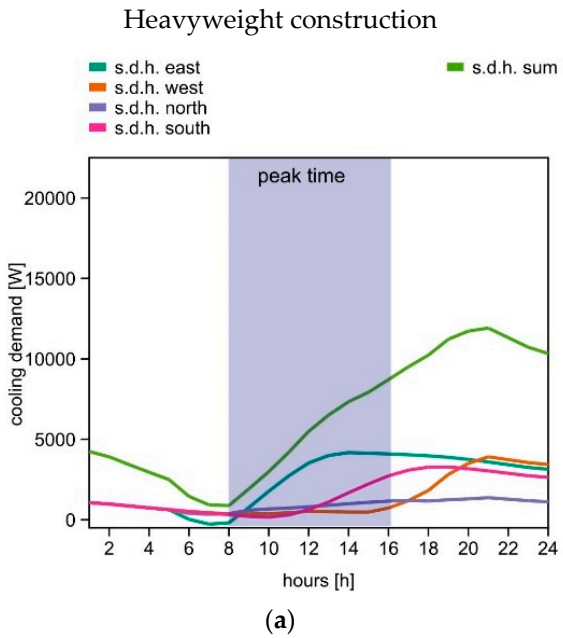


(**a**)

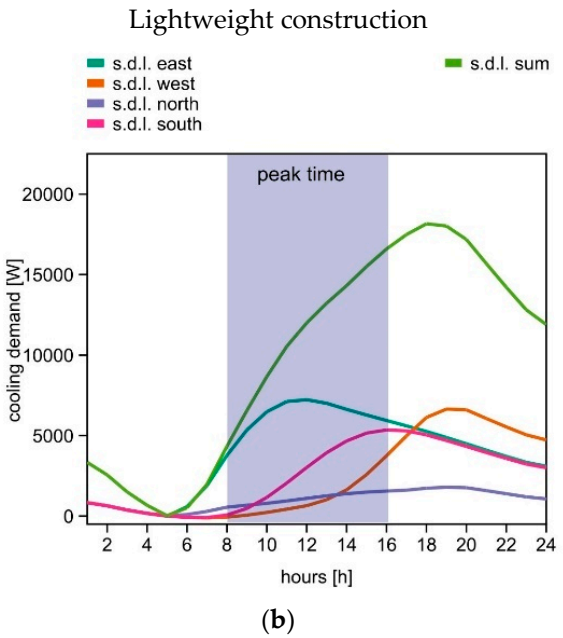


(**b**)

**Figure 9.** *Cont.*

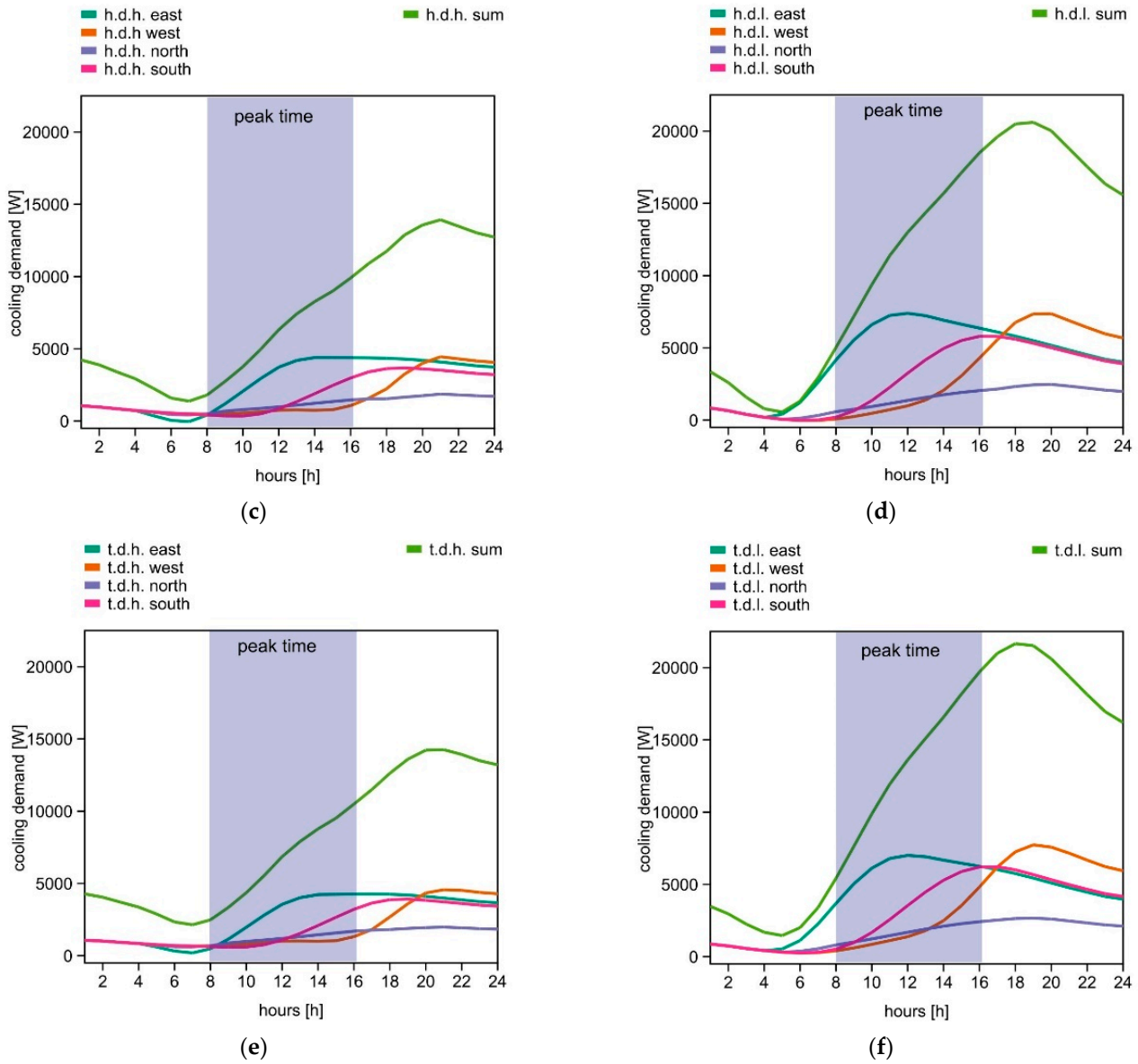


**Figure 9.** (**a**–**f**) Cooling demand of sample building at different orientations in the case of summer, hot, and torrid days.

**Table 13.** Cooling demand rate in lightweight construction [%].

| | Summer Day | Hot Day | Torrid Day |
|---|---|---|---|
| All day | 100.0 | 113.8 | 118.2 |
| Peak time (8 a.m.–4 p.m.) | 89.3 | 99.6 | 105.9 |
| Difference | 10.7 | 14.2 | 12.3 |

It can also be seen in Tables 13 and 14 that the percentage rate of cooling demand on a summer day is very similar in both types of buildings. However, during peak time, the percentage rate shows a big difference due to the heat storage capacity. The difference in the cooling demand between the investigated periods (peak time period of the investigated days) is between 10.7 and 14.2% for lightweight construction, while for heavyweight construction, it is between 31.2 and 35.8%, as can be seen in Tables 13 and 14.

**Table 14.** Cooling demand rate in heavyweight construction [%].

| | Summer Day | Hot Day | Torrid Day |
|---|---|---|---|
| All day | 100.0 | 114.8 | 115.9 |
| Peak time (8 a.m.–4 p.m.) | 68.8 | 79.0 | 83.6 |
| Difference | 31.2 | 35.8 | 32.3 |

The maximum heat load value of the buildings will apply after the peak time. The differences between the highest cooling demand value during the peak time and the maximum cooling demand value during the day are significantly higher in the case of a heavyweight building than in the cases of a lightweight building because the thermal capacity of the buildings influences the cooling load on hotter days, as can be seen in Table 15.

**Table 15.** Cooling demand rate differences [%].

| Cooling Demand Rate | Lightweight Construction | | | Heavyweight Construction | | |
|---|---|---|---|---|---|---|
| | Summer Day | Hot Day | Torrid Day | Summer Day | Hot Day | Torrid Day |
| All day | 100% | +13.8% | +18.2% | −33.1% | −23.2% | −22.5% |
| Peak time (8 a.m.–4 p.m.) | −10.7% | −0.4% | +5.9% | −54.0% | −47.7% | −44.1% |

By comparing lightweight and heavyweight building constructions, our study highlights how differences in thermal capacity affect cooling load and peak demand times. This addresses a gap in the literature, which has traditionally focused on general construction or operational metrics without distinguishing the unique cooling behaviors of these materials. Our findings show that heavyweight constructions have higher cooling demands later in the day, while lightweight structures peak earlier, and these insights should inform design choices for energy-efficient, comfort-oriented HVAC systems. This study also identifies how room orientation significantly affects cooling needs, especially in buildings with large, glazed surfaces. By linking cooling demand to specific orientations and occupancy schedules, we offer guidance for HVAC system optimization that goes beyond existing recommendations, which often do not account for such detailed operational nuances. These data can be leveraged to allocate building spaces strategically and design HVAC systems that align with peak usage periods, reducing overall energy consumption. This study's insights are highly applicable to architects, HVAC system designers, and building managers who are responsible for ensuring energy efficiency and occupant comfort, especially in commercial and public buildings. By providing data-driven recommendations on structural orientation and occupancy planning, our study aids in designing and operating HVAC systems that minimize cooling costs and environmental impact while maximizing comfort during peak summer conditions.

## 4. Conclusions

In the present article, the external air temperature and its relations to frequency of occurrence, heat waves, summer, hot, and torrid days were analyzed (782 days in total). In addition, for the analyzed days, the effect of the "clear sky" on the radiation was considered. Unfortunately, most of the comfort and energy standards do not contain external meteorological data. In this paper, actual summer, hot, and torrid days were chosen, then the raw data were adjusted to a clear sky day, and the EN ISO 13790:2008 was used for the calculations. When calculating the cooling load for different operative temperatures, it is essential to know the values and variations of the external air temperature and solar radiation.

It can be observed that the cooling demand of a building depends on the orientation of its transparent surfaces and the type of construction (i.e., heavyweight or lightweight).

1. The results of our calculations on peak-time cooling performance show a significant difference between the peak cooling performance requirements of light- and heavyweight buildings. This is due to the different thermal capacities of the structures. As the thermal resistances of the structures are the same, the difference between the building structures is how the direct solar gain is handled. This difference is particularly significant when maintaining operative temperature conditions. The impact is less pronounced when only air temperature is maintained.
2. Based on the investigated meteorological data, the used sample days in the Romanian standards are closer to an actual torrid day. The sample day used by the MSZ 04-140-2 standard [32] is closer to a summer day and underestimates the solar radiation values. It causes a relevant difference in the results of the calculation, especially in buildings with large transparent surfaces.
3. The peak operational period of the building greatly influences the amount of energy consumed. Taking into consideration both energy and human factors, the examined peak working hours from 8 a.m. to 4 p.m. represent an appropriate compromise. Based on calculations, it is advisable to minimize the building's use during the 4 p.m. to 7 p.m. time interval, especially in the case of buildings with west-facing, large-sized transparent surfaces. This investigation focused on the cooling demand during the peak time (8 a.m.–4 p.m.) as several buildings operate in this period.
4. When allocating spaces for various functions, it is essential to consider the analysis based on cardinal directions. By examining the peak usage times of specific spaces, it becomes possible to avoid the external heat load peak of the building and to reduce the amount of cooling energy consumed. The rooms with transparent surfaces facing north have the lowest cooling demand in all cases. At peak time, the rooms with east-facing transparent surfaces have the highest cooling demand.

In the future, the number of heat waves and the number of summer, hot, and torrid days is expected to increase, especially in the urban environment (heat island effect); thus, the investigation of the buildings within these external parameters is relevant.

**Author Contributions:** All authors listed have significantly contributed to the development and the writing of this article. All authors have read and agreed to the published version of the manuscript.

**Funding:** Project no. TKP2021-NKTA-34 has been implemented with the support provided from the National Research, Development and Innovation Fund of Hungary, financed under the TKP2021-NKTA funding scheme.

**Data Availability Statement:** The data that have been used are confidential.

**Acknowledgments:** The authors would like to express their gratitude to the Meteorological Observatory (Centre for Precision Farming R&D Services Faculty of Agriculture), Debrecen, for providing indispensable meteorological data. The copyright of the content quoted from the standards contained in the article is owned by the Hungarian Standards Institution (MSZT), and they are included here with the permission of the MSZT. Before applying the standards, make sure that the relevant standard has been amended, corrected, or withdrawn.

**Conflicts of Interest:** The author declares no conflicts of interest.

## Nomenclature

| | |
|---|---|
| $H_{ve}$ | Heat transfer by ventilation (W/K) |
| $\theta_{air}$ | Air temperature node (°C) |
| $\theta_{sup}$ | The supply temperature (°C) |
| $H_{tr,w}$ | Heat transfer by transmission is split into the window segment, (W/K) |
| $H_{tr,op}$ | The thermal mass (W/K) |
| $\theta_s$ | (A mix of $\theta_{air}$ and mean radiant temperature) and the node representing the mass of the building zone, $\theta_m$ (°C) |

| | |
|---|---|
| $C_m$ | Thermal capacity (J/K) |
| $\Phi_{int}$ | Heat flow rate given by internal heat sources (W) |
| $\Phi_{sol}$ | Solar heat sources (W) |
| $\Phi_{HC}$ | Energy need for cooling (W) |
| $A_f$ | The conditioned area ($m^2$) |
| $\theta_{air,10}$ | The air temperature obtained for a heating power of 10 W/$m^2$ (°C) |
| $\theta_{air,0}$ | Air temperature in free floating conditions (°C) |
| $\theta_{air,set}$ | Air temperature (°C) |
| S | Summer day |
| H | Hot day |
| T | Torrid day |
| $I_{GH}$ | Is the global solar radiation on horizontal surfaces (W/$m^2$) |
| $I_{dirH}$ | Direct solar radiation on horizontal surfaces (W/$m^2$) |
| $I_{difH}$ | Diffuse solar radiation on horizontal surfaces (W/$m^2$) |
| $I_{difV}$ | Diffuse solar radiation on vertical surfaces (W/$m^2$) |
| | Direct solar radiation on vertical surfaces (W/$m^2$) |
| $I_{dirSouth}$, $I_{dirEast}$, | Direct solar radiation on vertical surfaces (W/$m^2$) |
| $I_{dirWest}$, $I_{dirNorth}$ | Direct solar radiation on vertical surfaces (W/$m^2$) |
| | Direct solar radiation on vertical surfaces (W/$m^2$) |
| $k_T$ | The clearness index |
| $G_{SC}$ | The solar constant (W/$m^2$) |
| $\theta_z$ | The zenith angle of the sun (°) |
| $\theta$ | The incidence angle (°) |
| $\delta$ | The solar declination (°) |
| $\varphi$ | The latitude (°) |
| $\beta$ | The angle of the surface with horizontal (°) |
| $\gamma$ | The solar azimuth angle (°) |
| $\omega$ | The hour angle (°) |
| $n$ | The number of the analyzed day of the year |
| $R_b$ | Geometrical factor |

## References


1. Owen, M.S.; Kennedy, H.E. *ASHRAE Handbook: Fundamentals American Society of Heating, Refrigeration, and Air-Conditioning Engineers*; ASHRAE: New York, NY, USA, 2009.
2. ASHRAE. *Cooling and Heating Load Calculation Manual American Society of Heating, Refrigeration, and Air-Conditioning Engineers*; ASHRAE: New York, NY, USA, 1979.
3. *ISO 52000-1:2017(en)*; Energy Performance of Buildings—Overarching EPB Assessment—Part 1: General Framework and Procedures. ISO: Geneva, Switzerland, 2017.
4. *EN ISO 13790:2008*; Energy Performance of Buildings—Calculation of Energy Use for Space Heating and Cooling. European Committee for Standardization: Brussels, Belgium, 2008.
5. Palme, M.; Isalgué, A.; Coch, H. Avoiding the Possible Impact of Climate Change on the Built Environment: The Importance of the Building's Energy Robustness. *Buildings* **2013**, *3*, 191–204. [CrossRef]
6. Antoniadou, P.; Papadopoulos, A.M. Occupants' thermal comfort: State of the art and the prospects of personalized assessment in office buildings. *Energy Build.* **2017**, *153*, 136–149. [CrossRef]
7. Wang, X.; Chen, D.; Ren, Z. Assessment of climate change impact on residential building heating and cooling energy requirement in Australia. *Build Environ.* **2010**, *45*, 1663–1682. [CrossRef]
8. Huang, K.-T.; Hwang, R.-L. Future trends of residential building cooling energy and passive adaptation measures to counteract climate change: The case of Taiwan. *Appl. Energy* **2016**, *184*, 1230–1240. [CrossRef]
9. Hacker, J.N. Modelling passive and active cooling strategies for housing under present and projected future climate—A case study of London. In Proceedings of the 5th Windsor Conference: Air Conditioning and the Low Carbon Cooling Challenge, Windsor, UK, 27–29 July 2008; NCEUB: London, UK, 2008; pp. 27–29.
10. Woradechjumroen, D.; Yu, Y.; Li, H.; Yu, D.; Yang, H. Analysis of HVAC system oversizing in commercial buildings through field measurements. *Energy Build.* **2014**, *69*, 131–143. [CrossRef]
11. Djunaedy, E.; Van den Wymelenberg, K.; Acker, B.; Thimmana, H. Oversizing of HVAC system: Signatures and penalties. *Energy Build.* **2011**, *43*, 468–475. [CrossRef]
12. Szabó, L.G.; Kalmár, F. Parametric Analysis of Buildings' Heat Load Depending on Glazing: Hungarian Case Study. *Energies* **2018**, *11*, 12. [CrossRef]

13. Csáky, I.; Kalmár, F. Effects of thermal mass, ventilation and glazing orientation on indoor air temperature in buildings. *J. Build. Phys.* **2015**, *39*, 189–204. [CrossRef]
14. Csáky, I.; Kalmar, F. Effects of solar asymmetry on building's cooling energy needs. *J. Build. Phys.* **2015**, *1*, 35–54. [CrossRef]
15. Csáky, I.; Kalmár, F. Investigation of the relationship between the allowable transparent area, thermal mass and air change rate in buildings. *J. Build. Eng.* **2017**, *12*, 1–7. [CrossRef]
16. Csáky, I. Analysis of Daily Energy Demand for Cooling in Buildings with Different Comfort Categories: Case Study. *Energies* **2021**, *14*, 4694. [CrossRef]
17. Csima, G.; Horányi, A. Validation of the ALADIN-Climate regional climate model at the Hungarian Meteorological Service. *Időjárás* **2008**, *112*, 155–177.
18. Bottyán, Z.; Kircsi, A.; Szegedi, S.; Unger, J. The relationship between built-up areas and the spatial development of the mean maximum urban heat island in Debrecen, Hungary. *Int. J. Climatol.* **2005**, *25*, 405–418. [CrossRef]
19. Hungarian Meteorological Services. Evaluation of Extreme Climate Indices. Available online: http://www.met.hu/en/omsz/tevekenysegek/klimamodellezes/szelsosegek/ (accessed on 18 June 2022).
20. Debbage, N.; Shepherd, J.M. The urban heat island effect and city contiguity. *Comput. Environ. Urban Syst.* **2015**, *54*, 181–194. [CrossRef]
21. *Heat Wave | Meteorology*; Encyclopedia Britannica: Edinburgh, UK, 1 April 2019.
22. Erbs, D.G.; Klein, S.A.; Duffie, J.A. Estimation of the diffuse radiation fraction for hourly, daily and monthly-average global radiation. *Sol. Energy* **1982**, *28*, 293–302. [CrossRef]
23. Duffie, J.A.; Beckman, W.A. *Solar Engineering of Thermal Processes*, 3rd ed.; John Wiley & Sons Inc.: Hoboken, NJ, USA, 2006.
24. Clemens, J. Entwicklung Eines Einfachen Modells zur Abschätzung der Sommerlichen Überwärmung in Gebäuden. Diplomarbeit. Universität-Gesamthochschule Siegen, Fachbereich Physik: Siegen, Germany, 2000. Available online: http://nesa1.uni-siegen.de/download/Diplomarbeit_Clemens.pdf (accessed on 12 November 2024).
25. Basunia, M.A.; Yoshio, H.; Abe, T. Simulation of Solar Radiation Incident on Horizontal and Inclined Surfaces. *J. Eng. Res. (TJER)* **2012**, *9*, 27–35. [CrossRef]
26. Dragicevic, S.; Vuckovic, N. Evaluation of Distributional Solar Radiation Parameters of Cacak Using Long–Term Measured Global Solar Radiation Data. *Therm. Sci.* **2007**, *11*, 125–134. [CrossRef]
27. Hsieh, J.S. *Solar Energy Engineering*; Prentice-Hall: Englewood Cliffs, NJ, USA, 1986.
28. Barótfi, I. *Environmental Technology (in Hungarian)*; Mezőgazda Kiadó: Budapest, Hungary, 2000.
29. Bogoslovskij, B.N.; Poz, M.J. *Teplofizika Apparatov Utilizatii Tepla System Otoplenija, Ventilatii i Konditionirovania Vazduha*; Stroizdat: Moskva, Russia, 1983.
30. Kondratev, K.J.; Povovarova, Z.M.; Fedorova, M.P. *Radiationnij Rejim Naklonnih Poverhnostej*; Gidrometeoizdat: Saint Petersburg, Russia, 1978; p. 340.
31. Norris, D.J. Solar Radiation on Inclined Surfaces. *Sol. Energy* **1966**, *10*, 72–76. [CrossRef]
32. Liu, B.Y.H.; Jordan, R.C. Daily Insolation on Surface Tilted Towards the Equator. *ASHRAE J.* **1961**, *3*, 53–59.
33. Hongda, L.; Lun, L.; Yang, H.; Fang, L. Method of identifying the lengths of equivalent clear-sky periods in the time series of DNI measurements based on generalized atmospheric turbidity. *Renew. Energy* **2019**, *136*, 179–192. [CrossRef]
34. Urban INCD Incerc, Minister of Regional Development and Tourism. *Statistics os Romania Meteorological Data for Air Conditioning Equipment*; Contract nr. 483/2011; Ministry of Regional Development and Tourism: Bucharest, Romania, 2011.
35. *MSZ 04-140-2*; Power Engineering. Dimensioning Calculuses of Buildings and Building Envelope Structures. Hungarian Standard Commitment: Budapest, Hungary, 1992.
36. *MSZ CR 1752:2000*; Ventilation for Buildings. Hungarian Standard Commitment: Budapest, Hungary, 2000.